Self-Calibration Adjustment of CBERS-02B Long-Strip Imagery

Maoteng Zheng, Yongjun Zhang, Junfeng Zhu, and Xiaodong Xiong

Abstract—Due to hardware limitations, such as the poor accuracy of its onboard Global Positioning System receiver and star tracks, the direct georeferencing accuracy of the China and Brazil Earth Resource Satellite 02B (CBERS-02B) by its onboard position and attitude measurements is less than 1000 m at times. Thus, the image data cannot be directly used in surveying applications. This paper presents a self-calibration bundle adjustment strategy to improve the georeferencing accuracy of the onboard high-resolution camera (HRC). An adequate number of automatically matched ground control points (GCPs) are used to perform the bundle adjustment. Both the systematic error compensation model and the orientation image model along with the interior self-calibration parameters are used in the bundle adjustment to eliminate the systematic errors. A self-calibration strategy is used to compensate for the time delay and integrated charge-coupled device translation and rotation errors by introducing a total of ten interior orientation parameters. The preliminary results show that the accuracy of self-calibration bundle adjustment is two pixels better than that of bundle adjustment without self-calibration, and the planimetric accuracy of the check points is about 10 m. The unusual variations of the exterior orientation parameters in some cases are eliminated after enlarging the orientation image intervals and increasing the weights of the onboard position and attitude observations.

Index Terms—Bundle adjustment, China and Brazil Earth Resource Satellite 02B (CBERS-02B), high-resolution camera (HRC), self-calibration.

I. INTRODUCTION

THE resolution of satellite imagery has been largely improved to 1 m or better in recent years. For example, the ground sample distances (GSDs) of IKONOS [1] and Quick-Bird [2], [28] at nadir have been reported to be 1.0 and 0.61 m, respectively; WorldView-2 [3], [29] has a GSD of 0.46 m (re-

M. Zheng is with the National Engineering Research Center of Geographic Information System, China University of Geosciences, Wuhan 430074, China (e-mail: tengve@whu.edu.cn).

Y. Zhang and X. Xiong are with the School of Remote Sensing and Information Engineering, Wuhan University, Wuhan 430079, China (e-mail: zhangyj@whu.edu.cn; xd_xiong@whu.edu.cn).

J. Zhu is with the Institute of Photogrammetry, Chinese Academy of Surveying and Mapping, Beijing 100830, China (e-mail: junfeng_zhuCASM@163.com).
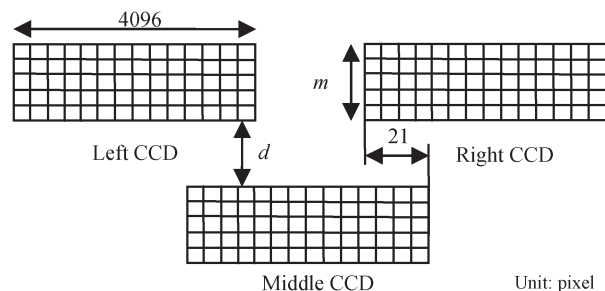
Fig. 1. Designed distribution of the TDI-CCD arrays on the focal plane of the CBERS-02B HRC.

sampled to 0.5 m as required by the government of the United States) at nadir; and GeoEye-1 [4] has a GSD of 0.41 m (resampled to 0.5 m for the same reason above), which is currently the highest resolution among all commercial satellites in the world. All of the above satellites adopted the linear pushbroom imaging mode to acquire high-quality linear-array imagery while integrated with high-accuracy Global Positioning System (GPS) receivers and star trackers to measure its instantaneous position and attitude data at the imaging time. These auxiliary data are transferred to a ground station and are used to perform direct georeferencing. The accuracy of direct georeferencing can achieve 3 m using the auxiliary data of GeoEye-1 [4].

The China and Brazil Earth Resource Satellite 02B (CBERS-02B) is the first high-resolution Earth observation satellite in China. It was launched on September 19, 2007, and has remained operational until now. The orbit height is about 780 km. The nadir ground resolution of the onboard high-resolution camera (HRC) is about 2.36 m, and the nominal focal length of the HRC is about 3300 mm. The time delay and integrated charge-coupled device (TDI-CCD) scanning mode, which is widely used in Earth observation satellites such as IKONOS, is also applied in the HRC of the CBERS-02B satellite [5], [6]. The TDI-CCD device has a high signal-to-noise ratio and good sensitivity, but the internal construction and optical geometry are more complicated than a conventional CCD unit, which leads to the difficulty encountered in data processing. A TDI-CCD device is actually a matrix array that consists of m lines of CCD arrays, where m is the number of CCD lines. However, in the TDI scanning mode, the concept of frames does not exist because the CCD lines are designed for imaging the same corresponding line on the ground at different times. The m CCD units at the same column will, in turn, image the same ground object, and the output signal will be amplified by accumulating all the signals that are captured by the m CCD units. The geometry of the TDI-CCD alignment, as shown in Fig. 1, is composed of three TDI-CCD devices installed on the left, middle,

and right of the focal plane, respectively; and each of them has 4096 pixels. The overlap of adjacent TDI-CCDs is 21 pixels. The middle TDI-CCD is shifted at a distance of d against the other two. The pixel size is 0.01 mm, the entire mosaicked CCD array width is 12 246 pixels, and the ground swath is 28.9 km.

The accuracy of direct georeferencing with the auxiliary data of CBERS-02B is usually about 1000 m, which does not meet the requirements of mapping applications [7]. A few ground control points (GCPs) are needed in the bundle adjustment to improve the geopositioning accuracy. Exterior orientation models for the bundle adjustment with linear-array satellite imagery can be categorized into two classes, namely, generic models and strict physical models. A generic model is often referred to as a rational function model. It is actually a mathematical function that is adopted to model the relationship between the image coordinates and the object coordinates [2], [8]–[10]. It is simple and fast but is not suitable for the geolocation of long-strip imagery or sensor geometric calibration. A strict physical model uses exterior orientation parameters (EOPs) and interior orientation parameters (IOPs) to represent a sensor's instantaneous position, attitude, and camera geometry parameters at the time of scanning [11]. The ground object coordinates can be calculated with these EOPs, IOPs, image coordinates, and digital elevation model (DEM), according to the collinearity condition. Bundle adjustment is generally used to recover all these parameters. Since we are dealing with linear-array imagery, a proper trajectory model must be adopted to represent the EOPs' variations by time and reduce the number of unknown parameters. Several trajectory models, such as the quadratic polynomial model [12], the systematic error compensation model [13], the orientation image model [13]–[16], and the piecewise polynomial model [11], [16]–[18], are widely used. Some researchers also use rigorous models with orbit mechanics constraint [19], [20]. As for 02B imagery, Yue *et al.* [5] adopted a quadratic polynomial model to perform the bundle adjustment. Marcato and Tommaselli [6] combined the control points and lines with orbital data to perform exterior orientation.

On-orbit sensor calibration is a significant procedure before the mapping application, such as SPOT5 [21], [26], ALOS [22], [27], and Orbview-3 [23]. Since the internal construction of the TDI-CCD devices in CBERS-02B HRC is complicated, the IOPs must be introduced into the bundle adjustment to eliminate the misalignment error of the TDI-CCD devices and to improve the georeferencing accuracy [7]. Yue *et al.* [5] introduced three translation parameters along track that correspond to the left, middle, and right TDI-CCDs, respectively. However, this scheme can only eliminate the TDI-CCD translation errors along track; the systematic errors across track still exist. There may also be a rotation angle between the real position and the designed position of the TDI-CCD devices. Moreover, the CCD size error and the CCD bending error also exist. These two types of errors are much smaller than the expected overall positional error based on GCP matching, and the accuracy of the automatically matched control points (about 3 m in planimetry and 10 m in height) is too low to identify these errors and therefore is ignored in this paper. The workflow of this method is shown in Fig. 2.
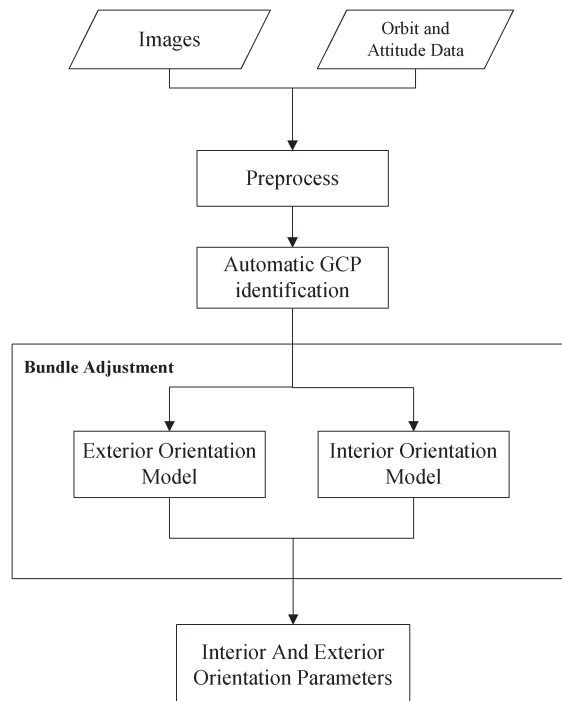

Fig. 2.   Workflow of on-orbit sensor calibration.

This work is further research based on an original study submitted to the 2012 International Society of Photogrammetry and Remote Sensing Conference in Melbourne, Australia [7]. The systematic error compensation model is combined with the orientation image model to perform the bundle adjustment, and the translation and rotation parameters are introduced to eliminate the TDI-CCD misalignment error. Ten parameters, including f (referring to the focal length) and $(\theta_l, \Delta x_l, \Delta y_l)$, $(\theta_m, \Delta x_m, \Delta y_m)$, and $(\theta_r, \Delta x_r, \Delta y_r)$, which refer to the corrections of the left, middle, and right CCDs, respectively, are introduced into the bundle adjustment with the long orbit data; these parameters may be correlated. A proper combination of these IOPs will be drawn according to these experiments. We enhanced the gross error detection and elimination algorithms of the GCPs, compared with the original work, due to the many gross errors in the automatically matched GCPs. The original findings (i.e., the calibration of the IOPs can improve the geopositioning accuracies, and there are relativities among the IOPs) are verified in this paper. The methods of enlarging the orientation image intervals and increasing the weights of the GPS and star tracker observations are applied to eliminate the unusual variations of the EOPs caused by gross errors and the lack of GCPs, as mentioned in the original work [7]. The accuracy of the bundle adjustment is improved to less than 10 m in planimetry by using our method. The detailed results are discussed in Section III.

II. METHODOLOGY

Exterior orientation and interior orientation are the key issues of geopositioning before map applications; the exterior orientation models (known to be trajectory models since we are dealing with linear imagery) and the interior orientation

model are used in this paper according to the characteristics of CBERS-02B HRC imagery.

A. Exterior Orientation Model

A proper trajectory model is needed to represent the EOPs' variations by time and to reduce the number of unknown parameters. All the EOPs can be calculated by these model parameters, which will be solved in the bundle adjustment. The quadratic polynomial model, the systematic error compensation model, the piecewise polynomial model, and the orientation image model are the most commonly adopted models, as discussed in Section I. In this paper, the systematic error compensation model is combined with the orientation image model for the bundle adjustment.

1) Systematic Error Compensation Model: The systematic errors of the position and attitude data can be described by the quadratic polynomials about time since the orbit and attitude of the satellite are usually very stable compared with airborne sensors, and the real position and attitude of the satellite are equal to the position and attitude observations plus the corresponding systematic errors, which are calculated by the quadratic polynomial parameters and the corresponding imaging time, as shown in the following equations:

$$
\begin{aligned}
Xs &= Xs_0 + \Delta Xs \\
Ys &= Ys_0 + \Delta Ys \\
Zs &= Zs_0 + \Delta Zs \\
\varphi &= \varphi_0 + \Delta\varphi \\
\omega &= \omega_0 + \Delta\omega \\
\kappa &= \kappa_0 + \Delta\kappa
\end{aligned} \tag{1}
$$

where $Xs, Ys, Zs, \varphi, \omega, \kappa$ are the satellite position and attitude; and $Xs_0, Ys_0, Zs_0, \varphi_0, \omega_0, \kappa_0$ are the onboard observations of the position and attitude of the sensor. $\Delta Xs, \Delta Ys, \Delta Zs, \Delta\varphi, \Delta\omega, \Delta\kappa$ are the systematic errors of the position and attitude of the sensor, i.e.,

$$
\begin{aligned}
\Delta Xs &= a_0 + a_1 t + a_2 t^2 \\
\Delta Ys &= b_0 + b_1 t + b_2 t^2 \\
\Delta Zs &= c_0 + c_1 t + c_2 t^2 \\
\Delta\varphi &= d_0 + d_1 t + d_2 t^2 \\
\Delta\omega &= e_0 + e_1 t + e_2 t^2 \\
\Delta\kappa &= f_0 + f_1 t + f_2 t^2
\end{aligned} \tag{2}
$$

where $a_0, b_0, c_0, d_0, e_0, f_0, a_1, b_1, c_1, d_1, e_1, f_1, a_2, b_2, c_2, d_2, e_2, f_2$ are the polynomial coefficients of the systematic error compensation model, and t is the time parameter.

2) Orientation Image Model: The EOPs of the orientation images at a certain time are treated as unknowns. The EOPs of each scanning line at the other times can be interpolated with the EOPs of the adjacent four orientation images, which will be solved in the bundle adjustment, i.e.,

$$
P(t_j) = \sum_{i=K-1}^{K+2} \left[P(t_i) \prod_{\substack{k=K-1 \\ k \neq i}}^{K+2} \frac{t - t_k}{t_i - t_k} \right] \tag{3}
$$

where $P(t_j), P(t_i)$ are the EOPs (referred to as $Xs, Ys, Zs, \varphi, \omega, \kappa$) at time t_j and t_i, t is the time of imaging, and t_k is the corresponding time of orientation image k.
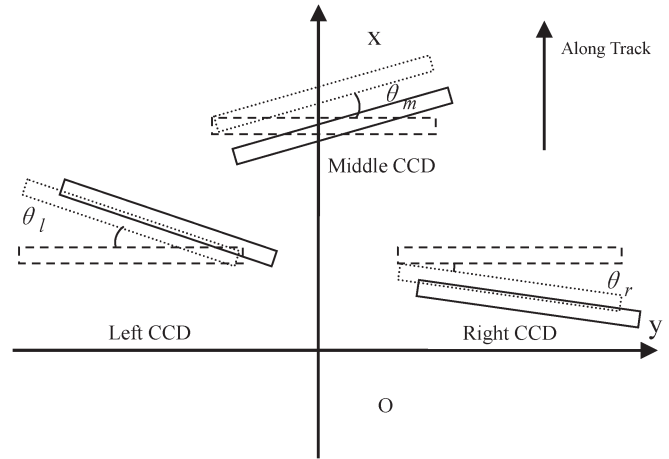

Fig. 3. CCD rotation and translation on the focal plane.

B. Calibration Model of Interior Parameters

In this paper, one rotation angle and two translation parameters of each of the left, middle, and right TDI-CCDs were introduced into the bundle adjustment as shown in Fig. 3. These parameters should be stable, but may change after operating for a long time in space; thus, it is suggested that the calibration process take place every one to two years.

The coordinates of the image points on the left, middle, and right TDI-CCDs can be calculated by the following equations:

$$
\begin{aligned}
x_l &= (n_l - c) \cdot \sin\theta_l \cdot p_x + x_{l0} + \Delta x_l \\
y_l &= -(n_m/2 + (n_l - c) \cdot \cos\theta_l) \cdot p_x + \Delta y_l \\
x_m &= (c - n_l) \cdot \sin\theta_m \cdot p_x + x_{m0} + \Delta x_m \\
y_m &= (-n_m/2 + (c - n_l) \cdot \cos\theta_m) \cdot p_x + \Delta y_m \\
x_r &= (c - n_l - n_m) \cdot \sin\theta_r \cdot p_x + x_{r0} + \Delta x_r \\
y_r &= (n_m/2 + (c - n_l - n_m) \cdot \cos\theta_r) \cdot p_x + \Delta y_r
\end{aligned} \tag{4}
$$

where O is the original point; x_l, y_l are the coordinates of the image points on the left subimage; x_m, y_m are the coordinates of the image points on the middle subimage; x_r, y_r are the coordinates of the image points on the right subimage; and x_{l0}, x_{m0}, x_{r0} are the distances between the left, middle, and right TDI-CCDs to the y-axis, which is determined by laboratory calibration. n_l, n_m are the pixel numbers of the left and middle TDI-CCDs; $\theta_l, \theta_m, \theta_r$ are the rotation parameters of the left, middle, and right TDI-CCDs; $\Delta x_l, \Delta y_l$ are the translation parameters of the left TDI-CCD; $\Delta x_m, \Delta y_m$ are the translation parameters of the middle TDI-CCD; $\Delta x_r, \Delta y_r$ are the translation parameters of the right TDI-CCD; c is the column index of image point; and P_x is the pixel size.

C. Error Equations of the Systematic Error Compensation Model

The error equations of the systematic error compensation model can be derived by (1) and (2) and can be written as

follows:

$$\mathbf{V_{img}} = \mathbf{Ax_{eop}} + \mathbf{Cx_{iop}} - \mathbf{l_{img}P_{img}}$$
$$\mathbf{V_{iop}} = \mathbf{x_{iop}} - \mathbf{l_{iop}P_{iop}} \quad (5)$$

$$\begin{bmatrix} \mathbf{V_{img}} \\ \mathbf{V_{iop}} \end{bmatrix} = \begin{bmatrix} \mathbf{A} & \mathbf{C} \\ \mathbf{O} & \mathbf{E} \end{bmatrix} \begin{bmatrix} \mathbf{x_{eop}} \\ \mathbf{x_{iop}} \end{bmatrix} - \begin{bmatrix} \mathbf{l_{img}} \\ \mathbf{l_{iop}} \end{bmatrix} \begin{matrix} \mathbf{P_{img}} \\ \mathbf{P_{iop}} \end{matrix} \quad (6)$$

where $\mathbf{X_{eop}}$ is the unknown vector of the systematic error compensation parameters; $\mathbf{X_{iop}}$ is the unknown vector of the IOPs; $\mathbf{l_{img}}$ is the discrepancy vector of the image point observations; $\mathbf{l_{iop}}$ is the discrepancy vector of the IOPs' pseudo-observations; $\mathbf{A}, \mathbf{C}$ are the design matrices; $\mathbf{O}$ is the zero matrix; $\mathbf{E}$ is the unit matrix; and $\mathbf{P_{img}}, \mathbf{P_{eop}}$ are the weights of the image point observations and the IOPs' pseudo-observations, respectively.

D. Error Equations of the Orientation Image Model

The error equations of the orientation image model can be derived by (3) and can be written as follows:

$$\mathbf{V_{img}} = \mathbf{Ax_{gps}} + \mathbf{Bx_{att}} + \mathbf{Cx_{iop}} - \mathbf{l_{img}P_{img}}$$

$$\mathbf{V_{gps}} = \mathbf{x_{gps}} - \mathbf{l_{gps}P_{gps}}$$

$$\mathbf{V_{att}} = \mathbf{x_{att}} - \mathbf{l_{att}P_{att}}$$

$$\mathbf{V_{iop}} = \mathbf{x_{iop}} - \mathbf{l_{iop}P_{iop}} \quad (7)$$

$$\begin{bmatrix} \mathbf{V_{img}} \\ \mathbf{V_{gps}} \\ \mathbf{V_{att}} \\ \mathbf{V_{iop}} \end{bmatrix} = \begin{bmatrix} \mathbf{A} & \mathbf{B} & \mathbf{C} \\ \mathbf{E} & \mathbf{O} & \mathbf{O} \\ \mathbf{O} & \mathbf{E} & \mathbf{O} \\ \mathbf{O} & \mathbf{O} & \mathbf{E} \end{bmatrix} \begin{bmatrix} \mathbf{x_{gps}} \\ \mathbf{x_{att}} \\ \mathbf{x_{iop}} \end{bmatrix} - \begin{bmatrix} \mathbf{l_{img}} \\ \mathbf{l_{gps}} \\ \mathbf{l_{att}} \\ \mathbf{l_{iop}} \end{bmatrix} \begin{matrix} \mathbf{P_{img}} \\ \mathbf{P_{gps}} \\ \mathbf{P_{att}} \\ \mathbf{P_{iop}} \end{matrix} \quad (8)$$

where $\mathbf{X_{gps}}$ is the unknown vector of the translation parameters; $\mathbf{X_{att}}$ is the unknown vector of the rotation parameters; $\mathbf{X_{iop}}$ is the unknown vector of the IOPs; $\mathbf{l_{img}}$ is the discrepancy vector of the image point observations; $\mathbf{l_{gps}}$ is the discrepancy vector of the GPS observations; $\mathbf{l_{att}}$ is the discrepancy vector of the star tracker observations; $\mathbf{l_{iop}}$ is the discrepancy vector of the IOPs' pseudo-observations; $\mathbf{A}, \mathbf{B}, \mathbf{C}$ are the design matrices; $\mathbf{O}$ is the zero matrix, $\mathbf{E}$ is the unit matrix; and $\mathbf{P_{img}}, \mathbf{P_{gps}}, \mathbf{P_{att}}$, and $\mathbf{P_{iop}}$ are the weights of the image point observations, the GPS observations, the star tracker observations, and the IOPs' pseudo-observations, respectively.

III. EXPERIMENT AND ANALYSIS

In this paper, the systematic error compensation model combined with the orientation image model was introduced into the bundle adjustment along with the IOPs. The systematic error compensation model was first used to eliminate the large systematic errors of the entire strip, and then, the orientation image model was utilized to eliminate the remained systematic errors. A best IOPs combination scheme was found after many test sequences with different combinations of these IOPs, as shown in Table II.

Since the position, the attitude observations, and the IOPs' pseudo-observations were introduced into the bundle adjustment, the best adjustment result was achieved while the proper weight matrix was fixed. The weights of all the observations
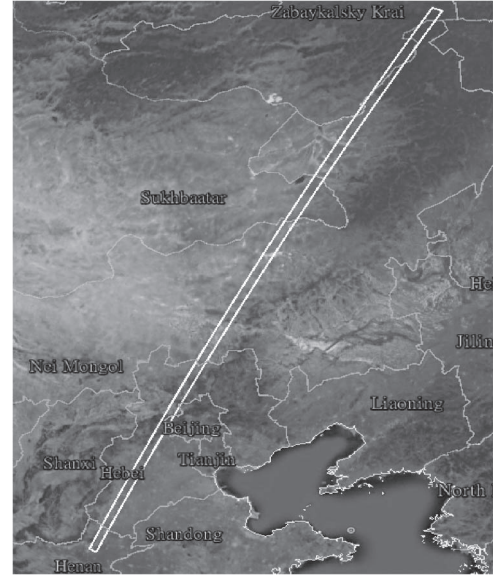

Fig. 4. White polynomial area is the ground coverage of the test block shown on Google Earth.

were fixed according to their priori accuracies, which were provided along with the metadata. The weights of the image points were set as the unit weight, and the weights of the other groups of observations were the square of the ratio of their accuracy and the image point accuracy. The weights of the IOPs' pseudo-observations were empirical values. The whole adjustment was performed in the WGS84 coordinate system, but the check point's root-mean-square error was transferred to the tangential plane coordinate system.

A real data set collected by the CBERS-02B HRC in December 2010 was used for the experiments in this paper. The test block consisted of only one strip, which covered an area of 28.9 km × 2284 km passing from Henan province to northeastern China, as shown in Fig. 4. The camera, as previously mentioned, utilizes three TDI-CCD devices to acquire linear imagery. The output image is mosaicked by three images that were acquired by the left, middle, and right TDI-CCD devices, but seams still exist in the mosaicked image, as shown in Fig. 5(a), and some CCD lines on the subimage are missing, as shown in Fig. 5(b).

A total number of 508 813 control points (about 5000 points per scene) were matched from 1:10 000 scale orthomaps, which is a standard digital ortho model (DOM) product provided by the official department of China, with a GSD of 2.5 m, and a public global DEM collected by Shuttle Radar Topography Mission (SRTM) using an automatic matching program developed by our research team. Half of them were used as independent check points in the bundle adjustment. The accuracies of these points were assessed to be about 3 m in planimetry and 10 m in height according to the reference orthomaps and SRTM. Some gross errors (mainly caused by the low contrast, weak texture, or other situation) existed among the control points. Thus, the gross error elimination procedure became inevitable during the bundle adjustment and was derived according to the posterior variance component estimation principle.
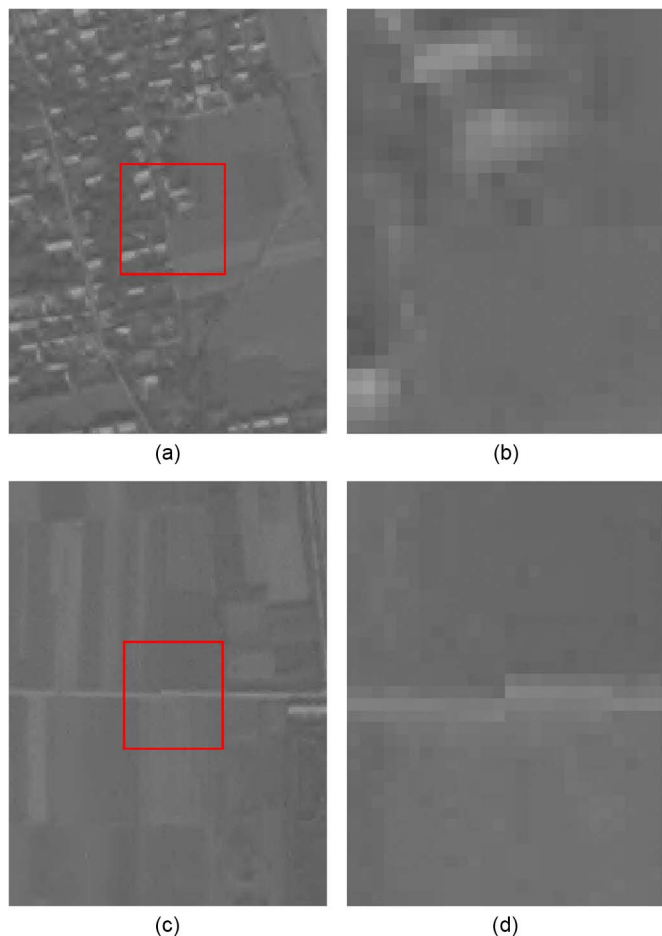
Fig. 5. (a) Missing scanner lines in the right CCD image. (b) Enlarged image of the rectangle area in (a). (c) Mosaic error between the left and middle CCD images. (d) Enlarged image of the rectangle area in (c).

TABLE I
IMAGE POINT RESIDUALS OF BUNDLE ADJUSTMENT WITH THE SUBIMAGES ACQUIRED BY THE LEFT, MIDDLE, AND RIGHT SUBIMAGES AND THE WHOLE IMAGE MOSAICKED BY THE THREE SUBIMAGES

Data source	Root Mean Square (RMS) of image points residuals (pixel)		Max absolute residuals of image points (pixel)	
	x	Y	x	y
Middle sub-image	1.8	2.3	6.7	-6.7
Left sub-image	1.9	2.2	-7.1	-6.9
Right sub-image	2.0	2.2	7.3	7.8
Whole image	4.5	4.0	24.3	-25.3

A. Bundle Adjustment With Three Subimages and the Mosaicked Image

The systematic error compensation model was first adopted to refine the EOPs, and then, the orientation image model was applied to eliminate the remaining systematic errors. As illustrated in Table I, the image point residuals of the bundle adjustment with the left, middle, or right subimages are two to three pixels less than that of the bundle adjustment with the whole image, which means that the whole image mosaicked by the three

TABLE II
IMAGE POINT RESIDUALS AND CHECK POINT PLANIMETRIC ACCURACY WITH DIFFERENT SCHEMES OF IOPs COMBINATIONS

ID	Parameters combinations	RMS of Image points residuals (pixel)		Max absolute residuals of image points (pixel)		RMS of Check points Residuals (m)	
		x	y	x	y	X	Y
1	f,x0,y0,a0,x1,y1,a1,x2,y2,a2	--	--	--	--	--	--
2	x0,y0,a0,x1,y1,a1, x2,y2,a2	--	--	--	--	--	--
3	f,x0,y0,a0 ,x2,y2,a2	1.1	1.8	4.2	-5.6	5.0	5.9
4	x0,y0,a0 ,x2,y2,a2	1.2	1.8	-4.4	5.7	4.7	5.8
5	f,x0,a0,x2,a2	1.3	2.0	-5.3	-6.0	5.3	6.9
6	x0,a0,x2,a2	1.3	1.9	-5.1	6.2	5.2	6.3
7	f,x0,y0,x2,y2	2.6	2.1	-8.1	-6.8	6.0	14.7
8	x0,y0,x2,y2	2.6	1.9	-8.2	5.8	6.2	14.7
9	f,x0,x2	2.7	2.1	8.4	-6.1	6.2	14.5
10	x0,x2	2.9	2.1	-8.3	6.5	6.1	15.0
11	No parameter	4.5	4.0	24.3	-25.3	8.0	23.2

subimages continues to have a misalignment error, and calibration of the interior parameters is necessary to eliminate the misalignment error caused by the rotation and translation of the TDI-CCD devices between the real and designed positions [24].

B. Bundle Adjustment With Different Combinations of IOPs

Ten IOPs, at most, were introduced into the adjustment: f refers to the focal length; x0, y0, a0 are the two translation parameters and one rotation parameter that refer to the left TDI-CCD; x1, y1, a1 are those of the middle TDI-CCD; and x2, y2, a2 are those of the right TDI-CCD. Among these ten parameters, (x0, y0, a0), (x1, y1, a1), and (x2, y2, a2) refer to the left, middle, and right TDI-CCDs, respectively; and these three groups of parameters are correlated to each other. We could not solve all of them in the same bundle adjustment process because they were nondeterminable if they were all set as unknowns. When one of them was fixed, the other two groups became determinable. This experiment was designed to investigate how these parameters contributed to the bundle adjustment, as well as which combination of them was the best.

The initial values of these parameters were fixed to be zero, except for focal length f, which was fixed to be the calibrated value in the laboratory, and all the values of these parameters changed as the bundle adjustment was in progress. The statistical results of the image point residuals and the independent check point's planimetric accuracy after bundle adjustment with different combinations of IOPs are shown in Table II.

As demonstrated in Table II and Fig. 6, the image point residuals and the check point's planimetric accuracy after bundle adjustment with seven IOPs (scheme 3 in Table II) were improved by a factor of 4, at most, compared with the scheme with no IOPs (scheme 11 in Table II). The adjustment did not converge, mainly because of the ill-conditioned near-singular normal matrix of the translation and rotation parameters, which referred to the left, middle, and right TDI-CCDs, all of which were set as unknowns (schemes 1 and 2 in Table II). Therefore,
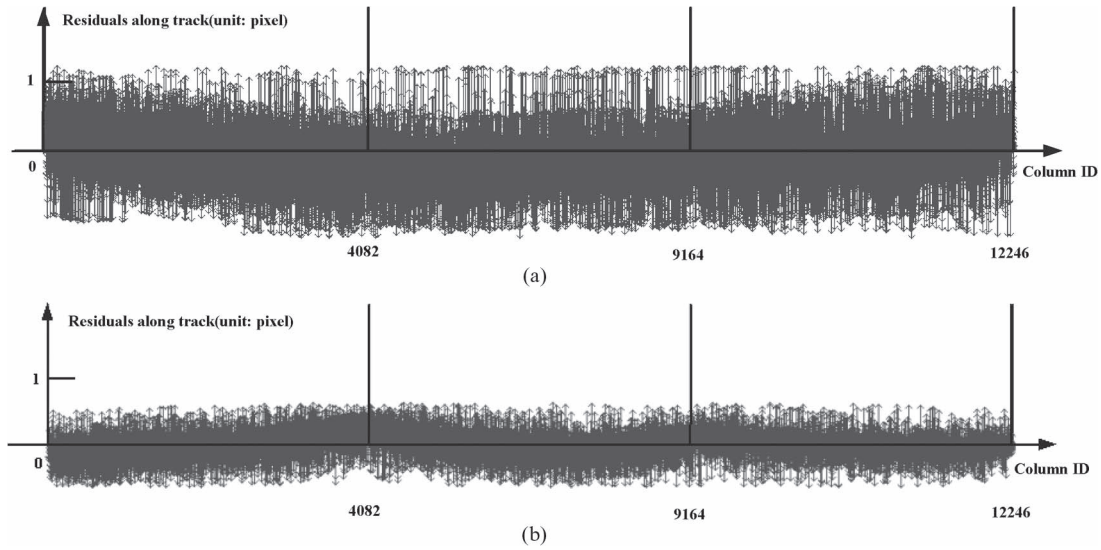
Fig. 6. Distribution of image point residuals with different schemes at the same scale. (a) Image point residuals with scheme 11 in Table II. (b) Image point residuals with scheme 3 in Table II.

the translation and rotation parameters (x1, y1, a1), which referred to the middle TDI-CCD, were not introduced in the adjustment (schemes 3 to 10 in Table II), although the middle TDI-CCD also may have had translation and rotation errors, but these errors might be compensated by the EOPs' translation and rotation parameters during the bundle adjustment since they are related to each other. As shown in schemes 5, 6, 7, and 8 in Table II, when the rotation parameters were introduced, the image point residuals in the x direction (along track) were reduced by 1.5 pixels, whereas the accuracy in the y direction (across track) did not change much. The planimetric accuracies of the check points were improved by one time in the Y direction, whereas there was no obvious improvement in the X direction. A rotation angle among these three CCD lines may exist according to the experiments. The focal length had no influence on the results, regardless of whether or not it was set as an unknown because it was correlated with the height unknowns of the EOPs and was effectively compensated by the EOPs.

We determined that the best combination of IOPs was scheme 3. (x0, y0, a0), (x1, y1, a1), and (x2, y2, a2) were nondeterminable while they were solved in the same bundle adjustment process, but two of them were determinable when the middle parameters were fixed, which agrees with the previous arguments. There was no absolute nondeterminable parameter; rather, all the parameters were determinable and became nondeterminable once they were solved together. The focal length parameter f was insignificant because the results differed very little with or without focal length f.

C. Relationship Among Orientation Image Intervals, Weights, and EOPs Variations

Since the GCPs were automatically matched from the reference orthomaps, a number of gross errors may have existed among them, and most of them were detected and removed during the bundle adjustment process. Thus, some areas with low contrast and weak texture, such as water and vegetation, had very few GCPs left, and the orientation images in these
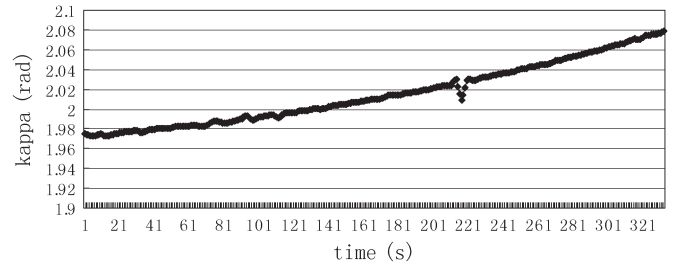

Fig. 7. Variation of the yaw angle of EOPs while orientation image interval is 3 s, where the horizontal axis represents the identity (ID) of the orientation image, and the vertical axis represents the value of the yaw angle (unit: radian).

areas were very unstable in the bundle adjustment. The weights of the position and attitude observations were increased, and the interval of the orientation images was enlarged to remove the influence caused by the gross errors in the GCPs. To further investigate the relationship between the orientation image interval and the EOPs' variations, the intervals of the orientation images were set by time, such as 3, 13, 20, 50, and 80 s, and the corresponding variation curves of the estimated yaw angle (kappa) of the EOPs in the bundle adjustment were as follows.

As shown in Fig. 7, the variation curve of the yaw angles of the EOPs undulated dramatically, particularly at time 221 while the interval of the orientation image was 3 s, which indicated that the orientation images in these areas were very unstable, mainly due to the gross errors or the lack of GCPs and a short orientation interval. In Fig. 8, the curve became smoother when the interval was enlarged to 13 s, but some small increases in the curve remained. In Fig. 9, it is shown that the increases almost disappeared when the interval was further enlarged to 20 s. In Figs. 10 and 11, as the interval was further enlarged to 50 and 80 s, the increases completely disappeared. The curve was very smooth, but it was not in accordance with the real trajectory of the attitude of the satellite, and the most proper interval appeared to be around 20 s.

The greater the contribution of the GCPs to the EOPs' unknowns of the orientation images during the bundle adjustment
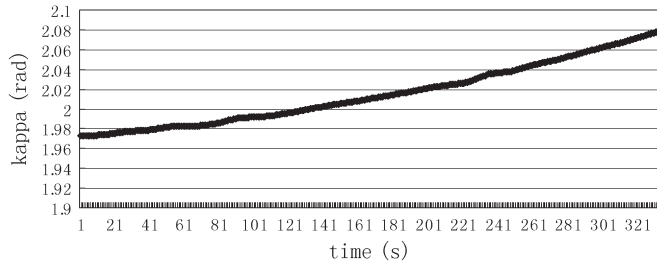
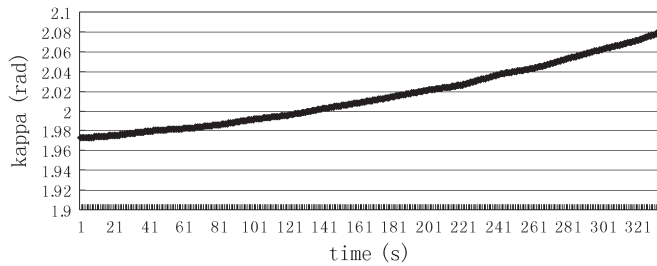Fig. 8. Variation of the yaw angle of EOPs with the interval of 13 s.

Fig. 9. Variation of the yaw angle of EOPs with an interval of 20 s.
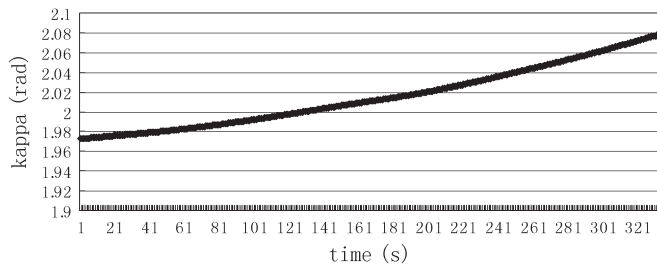

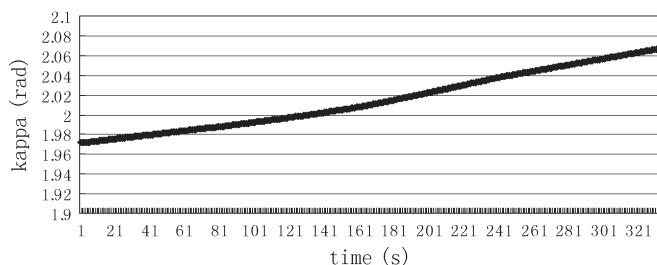Fig. 10. Variation of the yaw angle of EOPs with the interval of 50 s.

Fig. 11. Variation of the yaw angle of EOPs with the interval of 80 s.

when the interval of orientation images was enlarged, the greater was the possibility that the result would be more stable. On the other hand, the larger the orientation image intervals were, the greater was the probability that the model errors would be larger since it would not be oriented with the satellite orbit trajectory. Thus, proper orientation image intervals were necessary during the bundle adjustment, and according to the experimental results in this paper, 20 s is the proper interval.

IV. CONCLUSION

Different combinations of IOPs in the self-calibration bundle adjustment with CBERS-02B real data have been tested in this paper. The best scheme was found according to our test results. The geolocation accuracy was largely improved to about 5 m in

both directions of X and Y, which is a good outcome compared with the state-of-the-art research of CBERS-02B imagery [5]–[7]. Prior to this work, most of the applications with CBERS-02B imagery were restrained by the bad geolocation accuracy and small coverage of single scene. The main contributions of our method are its relatively high geolocation accuracy and large ground coverage while dealing with strip images. Our method also is more effective because the GCPs were all automatically matched without manual identification. The detailed findings follow.

The accuracy of the bundle adjustment with IOPs was improved by two to three pixels when compared with the bundle adjustment without IOPs, which indicates that it is reasonable to perform the bundle adjustment with self-calibration. The best results were obtained when only the translation and rotation parameters of the left and right CCDs were introduced, which also indicated that the ten IOPs were correlated to each other. Solving all of the ten parameters simultaneously could lead to an ill-conditioned near-singular normal matrix. If the translation and rotation parameters of the middle CCD are set as known, the other parameters can be confidently solved in the bundle adjustment.

The correlations between the IOPs and the EOPs always exist as long as they are solved in the same bundle adjustment process and are difficult to separate or identify. However, our main purpose was not to solve those correlations but rather to improve the geolocation accuracy, and we chose the best combination of parameters to make sure that the best geolocation accuracy was obtained.

Gross errors and the lack of GCPs will cause the calculation of EOPs to become unstable during the bundle adjustment, which can be effectively solved by enlarging the orientation image intervals and increasing the weights of the GPS and star tracker observations. Large GPS and star tracker observation weights would assure that the estimated EOPs will not end up with unreasonably large values [25]. However, the accuracy might be compromised because the resulting larger orientation image intervals may not align with the real satellite orbit trajectory. A proper interval is needed during the bundle adjustment procedure. The IOPs can be obtained after the bundle adjustment. However, the rectified orthoimage may have seam lines if the rotation angle parameters of the IOPs are significant. Therefore, these rotation parameters should be controlled by the weights of their pseudo-observations to ensure that they do not end up with large values after the bundle adjustment.

The proposed method can be used to process most of the high-resolution satellite data in China, such as the newly launched ZY02C and GF-1. The robustness and reliability of this method should be further verified when additional real data are available.

REFERENCES

[1] T. Toutin, "Error tracking in Ikonos geometric processing using a 3D parametric model," *Photogramm. Eng. Remote Sens.*, vol. 69, no. 1, pp. 43–51, 2003.

[2] X. Tong, S. Liu, and Q. Weng, "Bias-corrected rational polynomial coefficients for high accuracy geo-positioning of QuickBird stereo imagery," *ISPRS J. Photogramm. Remote Sens.*, vol. 65, no. 2, pp. 218–226, Mar. 2010.

[3] M. A. Aguilar, M. M. Saldaña, and F. J. Aguilar, "Assessing geometric accuracy of the orthorectification process from GeoEye-1 and WorldView-2 panchromatic images," *Int. J. Appl. Earth Observ. Geoinf.*, vol. 21, no. 2013, pp. 427–435, Apr. 2013.

[4] C. S. Fraser and M. Ravanbakhsh, "Georeferencing accuracy of GeoEye-1 imagery," *Photogramm. Eng. Remote Sens.*, vol. 75, no. 6, pp. 634–638, 2009.

[5] Q. X. Yue *et al.*, "The adjustment of CBERS-02B pan image," *Remote Sens. Land Resources*, vol. 79, no. 1, pp. 61–63, 2009.

[6] J. J. Marcato and A. M. G. Tommaselli, "Exterior orientation of CBERS-02B HRC imagery using multi-feature control and orbital data," *ISPRS J. Photogramm. Remote Sens.*, vol. 79, no. 2013, pp. 219–225, 2013.

[7] Y. J. Zhang and M. T. Zheng, "Bundle block adjustment with self-calibration of long orbit CBERS-02B imagery," *Int. Archives Photogramm., Remote Sens. Spatial Inf. Sci.*, vol. 39, part B1, pp. 291–296, 2012.

[8] C. S. Fraser and H. B. Hanley, "Bias-compensated RPCs for sensor orientation of high-resolution satellite imagery," *Photogramm. Eng. Remote Sens.*, vol. 71, no. 8, pp. 909–915, 2005.

[9] C. V. Tao and Y. Hu, "A comprehensive study of the rational function model for photogrammetric processing," *Photogramm. Eng. Remote Sens.*, vol. 67, no. 12, pp. 1347–1357, 2001.

[10] J. Grodecki and G. Dial, "Block adjustment of high-resolution satellite images described by rational polynomials," *Photogramm. Eng. Remote Sens.*, vol. 69, no. 1, pp. 59–68, 2003.

[11] D. Poli, "A rigorous model for spaceborne linear array sensors," *Photogramm. Eng. Remote Sens.*, vol. 73, no. 2, pp. 187–196, 2007.

[12] T. Kim and I. Dowman, "Comparison of two physical sensor models for satellite images: Position-rotation model and orbit-attitude model," *Photogramm. Rec.*, vol. 21, no. 114, pp. 110–123, 2006.

[13] Y. J. Zhang, M. T. Zheng, and T. Ke, "Triangulation of spaceborne three-line array imagery with different sensor models," in *Proc. Annu. Conf. ASPRS*, Milwaukee, WI, USA, 2011.

[14] H. Ebner, W. Kornus, and T. Ohlhof, "A Simulation Study on Point Determination for the MOMS-02/D2 space project using an extended functional model," *Int. Archives Photogramm. Remote Sens.*, vol. 29, part B4, pp. 458–464, 1992.

[15] C. S. Fraser and J. Shao, "Exterior orientation determination of MOMS-02 three-line imagery: Experiences with the Australian testified area," *Int. Archives Photogramm. Remote Sens.*, vol. 31, part B3, pp. 207–214, 1996.

[16] A. Grün and L. Zhang, "Automatic DTM generation from three-line-scanner (TLS) images," *Int. Archives Photogramm. Remote Sens.*, vol. 34, part 2A, pp. 131–137, 2002.

[17] O. Hofmann, P. Navé, and H. Ebner, "DPS—A digital photogrammetric system for producing digital elevation models and orthophotos by means of linear array scanner imagery," *Int. Archives Photogramm. Remote Sens.*, vol. 24, no. 3, pp. 216–227, 1982.

[18] V. Kratky, "Rigorous photogrammetric processing of SPOT images at CCM Canada," *ISPRS J. Photogramm. Remote Sens.*, vol. 44, no. 2, pp. 53–71, 1989.

[19] T. Ohlhof, O. Montenbruck, and E. Gill, "A new approach for combined bundle block adjustment and orbit determination based on Mars-94 three-line scanner imagery and radio tracking data," *Int. Archives Photogramm. Remote Sens.*, vol. 30, part 3, pp. 630–639, 1994.

[20] P. Michalis and I. Dowman, "A generic model for along-track stereo sensors using rigorous orbit mechanics," *Photogramm. Eng. Remote Sens.*, vol. 74, no. 3, pp. 303–309, 2008.

[21] W. Kornus, R. Alamús, A. Ruiz, and J. Talaya, "DEM generation from SPOT-5 3-fold along track stereoscopic imagery using autocalibration," *ISPRS J. Photogramm. Remote Sens.*, vol. 60, no. 3, pp. 147–159, 2006.

[22] J. Takaku and T. Tadono, "PRISM on-orbit geometric calibration and DSM performance," *IEEE Trans. Geosci. Remote Sens.*, vol. 47, no. 12, pp. 4060–4073, Dec. 2009.

[23] D. Mulawa, "On-orbit geometric calibration of the orbview-3 high resolution imaging satellite," *Int. Archives Photogramm., Remote Sens. Spatial Inf. Sci.*, vol. 35, part B1, pp. 1–6, 2004.

[24] Y. J. Zhang, M. T. Zheng, J. X. Xiong, Y. H. Lu, and X. D. Xiong, "On-orbit geometric calibration of ZY-3 three-line array imagery with multi-strip data sets," *IEEE Trans. Geosci. Remote Sens.*, vol. 52, no. 1, pp. 224–234. Jan. 2014.

[25] Y. J. Zhang, X. D. Xiong, X. Shen, and Z. Ji, "Bundle block adjustment of weakly connected aerial imagery," *Photogramm. Eng. Remote Sens.*, vol. 78, no. 9, pp. 983–989. 2012.

[26] A. Bouillon *et al.*, "SPOT 5 HRS geometric performances: Using block adjustment as a key issue to improve quality of DEM generation," *ISPRS J. Photogramm. Remote Sens.*, vol. 60, no. 3, pp. 134–146, 2006.

[27] F. Rottensteiner, T. Weser, A. Lewis, and C. S. Fraser, "A strip adjustment approach for precise georeferencing of ALOS optical imagery," *IEEE Trans. Geosci. Remote Sens.*, vol. 47, no. 12, pp. 4083–4091, Dec. 2009.

[28] H. Eisenbeiss, E. Baltsavias, M. Pateraki, and L. Zhang, "Potential of Ikonos and QuickBird imagery for accurate 3D point positioning, orthoimage and DSM generation," *Int. Archives Photogramm., Remote Sens. Spatial Inf. Sci.*, vol. 35, no. B3, pp. 522–528, 2004.

[29] T. Toutin, C. V. Schmitt, and H. Wang, "Impact of no GCP on elevation extraction from WorldView stereo data", *ISPRS J. Photogramm. Remote Sens.*, vol. 72, pp. 73–79, 2012.

Maoteng Zheng was born in 1987. He received the B.S. and Ph.D. degrees from Wuhan University, Wuhan, China, in 2009 and 2014, respectively.

He is currently a Postdoctoral Researcher of the National Engineering Research Center of Geographic Information System, China University of Geosciences, Wuhan. His research interests include space and aerial photogrammetry and combined bundle adjustment with multisource data sets.
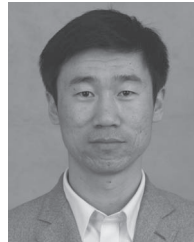
Yongjun Zhang was born in 1975. He received the B.S., M.S., and Ph.D. degrees from Wuhan University, Wuhan, China, in 1997, 2000, and 2002, respectively.

He is currently a Professor of photogrammetry and remote sensing with the School of Remote Sensing and Information Engineering, Wuhan University. His research interests include space, aerial, and low-attitude photogrammetry; image matching; combined bundle adjustment with multisource data sets; 3-D city reconstruction; and industrial inspection.

Junfeng Zhu was born in 1987. He received the B.S. and Ph.D. degrees from Wuhan University, Wuhan, China, in 2009 and 2014, respectively.

He is currently with the Chinese Academy of Surveying and Mapping, Beijing, China. His research interests include LiDAR data processing and aerial photogrammetry.

Xiaodong Xiong was born in 1987. He received the B.S. degree from Wuhan University, Wuhan, China, in 2009. He is currently working toward the Ph.D. degree in the School of Remote Sensing and Information Engineering, Wuhan University.

His research interests include LiDAR data processing and aerial photogrammetry.